Chapter 8

X-Ray Spectroscopy on Biological Systems

Joanna Czapla-Masztafiak, Wojciech M. Kwiatek,
Jacinto Sá and Jakub Szlachetko

Additional information is available at the end of the chapter

http://dx.doi.org/10.5772/64953

Abstract

In the field of biological studies, next to the standard methods, new tools are offered by contemporary physics. X-ray spectroscopic techniques enable probing electronic structure of occupied and unoccupied states of studied atom and distinguish the oxidation state, local geometry, and ligand type of elements that occur in biological material. Direct analysis using X-ray spectroscopy avoids many chemical preparation steps that might modify biological samples. The information obtained gives us insight into important biochemical processes all under physiological conditions. In this chapter we focus our attention to the application of X-ray spectroscopy to the study of biological samples, with special emphasis on mechanisms revealing interaction between DNA and different cytotoxic agents and in the determination of changes in oxidation state of different elements in pathologically altered human cells and tissue.

Keywords: X-ray spectroscopy, XAS, XES, DNA, chemical speciation

1. Introduction

X-ray spectroscopy is a powerful method giving the insight into the chemical and electronic structure of studied samples. Since twentieth century, it has been extensively used in a plethora or research fields starting from solid-state physics [1, 2] and followed by chemical [3] and environmental sciences [4], archeological and art research [5], as well as biological and health studies [6]. The advantages of this technique is its elemental specificity and high penetration depth of probe X-rays resulting in the possibility to undertake *in situ* experiments that provide information about the sample under ambient/operational conditions, that is, direct observation of species at the molecular level in low (biological) concentrations without the need for

preconcentration, extraction, or crystallization [7, 8]. For these reasons, X-ray spectroscopy has been recognized as the valuable addition to classical methods used in biological sciences and many improvements have been made in the experimental techniques as well as data analysis and interpretation. Research includes the simplest systems, such as single compounds, as well as more complex and heterogeneous structures such as cells and tissues. The examples of applications are, among others, the structural characterization of chloroperoxidase compound I [9], the determination of ligand environment of zinc in different tissues of Zn-hyperaccumulating plants [10] and chemical structure of metalloproteins [11]. A lot of researches concern changes in oxidation states of trace elements in case of different pathologically altered cells and tissues, for example the studies of differences in iron and zinc oxidation state contained in healthy and neoplastic tissues of the human brain [12], iron in normal and stenotic human aortic valves [13] or copper inside single neurons from Parkinson's disease and control substantia nigra [14]. Another group of application is identification of elements' chemical species in biological systems, like sulfur in erythrocytes and blood plasma [15], selenium in human cancer cells [16], as well as arsenic in various cell structures [17]. X-ray spectroscopy gives also the opportunity to follow biologically relevant processes in time-resolved experiments including the ultrafast time domain. The processes studied are for example excitation of Mn cluster in photosystem II [18] and recombination of myoglobin following the photolysis of NO [19]. The development of new X-ray sources and X-ray free electron lasers (XFELs) will make possible to study the dynamics of biological systems with femtosecond time resolution, which will elucidate the mechanisms of many important bioprocesses.

The need for more sensitive research methods in medical sciences is forced mostly by the increasing incidence rate of the diseases of affluence, primarily cancer and cardiovascular diseases [20]. These types of studies are focused on two main goals—effective diagnosis on the early stage of the disease and design of efficient therapy. This can be reached, for example, by the discovery and validation of new biomarkers to understand the etiopathology of diseases and by studying new, alternative treatment methods like, for example, novel potential drugs and their interaction with the components of living cells. This review summarizes our latest efforts in applying X-ray spectroscopy to study different biological systems starting from the impact of different damaging agents on the model of DNA molecule and followed by the chemical speciation in the studies of cancerous cell lines and human tissues. Chosen topics show the variety of medically important subjects that can be studied with X-ray spectroscopy and its undeniable role as a technique complementary to classical methods.

2. Principals of X-ray spectroscopy techniques

X-ray spectroscopic methods are atom-specific techniques, using X-ray excitation to gather information about the electronic and geometric structure of the studied system. X-rays in the range from several to few tens of keVs are absorbed by matter mainly through the photoelectric effect. In this process, an X-ray photon with sufficient energy is absorbed by an electron in a tightly bound quantum core level (such as the 1s, 2s or 2p) of an atom. A core electron is promoted to higher, unoccupied state or to the continuum. Following an absorption event, the

atom is in an excited state, with one of the core electron levels left empty (a core hole). During the decay of this intermediate excited state, the core hole is filled by another inner- or valence-shell electron. The decay from the excited to the final state is accompanied by the emission of an X-ray photon, which energy depends on electronic levels involved in the process or by the emission of an Auger electron or Coster-Kroning electron. But the latter phenomenon will not be discussed in this chapter. X-ray absorption and X-ray emission spectroscopy (XAS and XES, respectively) are devoted to the study aforementioned processes. XAS provides information about the unoccupied electronic density of states of an atom whereas XES reflects occupied density of states, and when applied together, providing the detailed picture of the molecular orbitals [21].

The absorption process is described by the absorption coefficient μ in the function of incidence energy, where we can distinguish two regions—a sharp rise in absorption (an absorption edge corresponding to the promotion of the core level electron to the higher state) and the region above absorption edge, characterized by the rich structure. Therefore, XAS spectrum is divided into two parts: the X-ray absorption near-edge structure (XANES)—typically within 30 eV of the main absorption edge, and the extended X-ray absorption fine-structure (EXAFS). XAS spectra are sensitive to the formal oxidation state, coordination chemistry, and the distances, coordination number, and species of the atoms surrounding the selected element. K- and L-level X-ray emission spectra, reflecting the energy distribution of photons emitted by the atoms, can be divided into α and β regions. α lines are characterized by high transition yields but provide little direct chemical information. On the other hand, β lines associated with satellites are being sensitive to chemical environment of the atom, but are much weaker in intensity. For example, two ranges may be recognized around X-ray emission spectrum of Kβ line: Kβ mainline consisting of metal 3p to metal 1s transitions and the valence-to-core (V2C K$\beta_{2,5}$) region comprised of transitions from valence, ligand-localized orbitals to the metal 1s. Both have been shown to contain valuable chemical information—the Kβ mainline is sensitive to the metal spin state as well as the metal-ligand covalence [22] while the V2C region contains information about ligand identity, electronic structure, and metal-ligand bond length [23].

The more detailed information about the electronic structure of studied systems can be obtained by the use of resonant X-ray emission spectroscopy (RXES, also called resonant inelastic X-ray scattering (RIXS)) that is characterized by high sensitivity. RXES, which is photon-in photon-out spectroscopy, combines X-ray absorption and X-ray emission information. RXES experiments can be performed with the use of high-energy resolution X-ray spectrometers, the powerful instruments used to determine the electronic structure of matter that have found many applications in a variety of scientific areas [24–28]. In general, X-ray spectrometers rely on the X-ray dispersion by a crystal providing high-energy resolution for X-ray detection. In order to access detailed information about the electronic structure of matter, the energy resolution has to be around 0.1–5 eV in order to be comparable with the natural lifetimes of studied electronic states of an atom [29, 30]. There are three relevant X-ray emission spectrometer geometries: von Hamos [31, 32], Johannson [33], and Johann [34]. In the RXES studies presented in this review, the von Hamos-type spectrometer has been used with segmented analyzer crystal which disperses the photon energy along one axis and focuses the

X-ray photons along the other axis [35]. Setup scheme for typical RXES experiment under physiological conditions is presented in **Figure 1**.

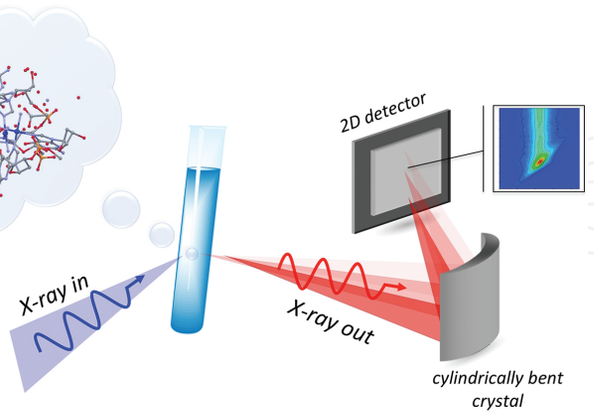

Figure 1. Schematic representation of the experimental setup used in *in situ* RXES experiment [7]. Reproduced by permission of The Royal Society of Chemistry.

The sample is placed at the center of the crystal curvature, and the X-rays are imaged on either a 1D strip detector or a 2D detector. This generates an emission spectrum in a single measurement without any detector or crystal motion. By scanning the incidence energy, one can obtain full RXES plane. A cut in the plane performed at maximum emission energy results in high-resolution X-ray absorption spectrum (HR-XAS) that, due to reduced lifetime broadening, provides detailed information about very small variations in the unoccupied electronic states. The example of RXES plane measured for cisplatin compound is presented in **Figure 2**. It shows the states generated by the resonant excitation of a $2p_{3/2}$ electron into the Pt 5d orbitals (L_3-edge transition). Schematically shown horizontal and vertical cuts along the RXES plane correspond to the $L\alpha_1$ lines of the X-ray emission spectrum (XES) and high-resolution X-ray absorption spectrum (HR-XAS) profiles, which provide information on occupied and unoccupied electronic states of the metal, respectively.

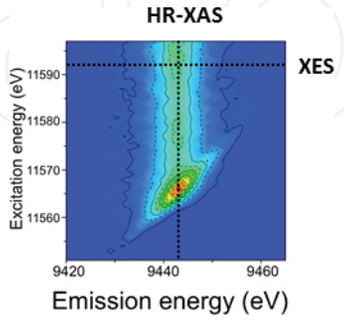

Figure 2. Pt L_3-edge RXES map of cisplatin compound [7]. Reproduced by permission of The Royal Society of Chemistry.

In parallel to the development of the experimental aspects of X-ray spectroscopy, the significant progress has been done in the theory and ab initio calculations of XAS and XES spectra that

enables detailed qualitative and quantitative analysis of experiment. Among others, two representatives of ab initio codes are FEFF9.0 [36] and FDMNES [37]. FEFF9.0, based on Green's Function, is automated software for ab initio multiple scattering calculations of X-ray absorption and X-ray emission signals and various other signals for solids, clusters, or molecules. The code provides yields for X-ray scattering amplitudes that may be directly compared to measured RXES signals. Recently, code was upgraded with several new features for more precise and more realistic calculations, which include ab initio Debye-Waller factors, improved treatment of inelastic loses and core-hole interaction as well as more accurate treatment of crystalline systems with k-space calculations of the Green's function. Similarly, to FEFF software, FDMNES provides yields for X-ray scattering amplitudes that may be directly compared to measured experimental spectra. Nevertheless, unlike FEFF, which is based on self-consistent spherical muffin-tin scattering potentials, the FDMNES employs the finite difference method (FDM) based on density functional theory (DFT) with a potential exchange correlation depending on the local electron density. Therefore, FDMNES may provide more accurate density of states calculations, especially for surface states, but at cost of much longer computation times.

3. Chemical analysis of antitumor compounds

It is beyond doubt that, in case of cancerous diseases, the effective therapy is needed. The majority of drugs used in cancer treatments are cytotoxic (cell killing) and interfere with the cells' DNA. Consequently, the DNA-drug interaction mechanism is of the primary interest when new antitumor compounds are studied. The development of new anticancer drugs is forced by the strong side effects and chemoresistance, both being induced when commonly used platinum-based chemotherapeutics are applied. The binding mechanism of newly synthesized complexes to DNA is one of the most important characteristics to be determined for identification of drug–DNA activity. This can be probed with direct techniques, like nuclear magnetic resonance (NMR) or crystallography. However, these approaches very often require harsh sample preparation that may lead to difficulties in the interpretation of the results. Therefore, simultaneously to the development of new routes of drug synthesis and studying drug-DNA interaction, further development of experimental techniques is necessary. Most importantly, detailed structural and electronic information of the samples has to be retrieved under *in situ* conditions with the ability to control the sample environment and mimicking real physiological conditions.

3.1. Chemical speciation

During the phase of designing new potential antitumor compound, it is important to understand how its structure influences its activity. Especially, it is essential to apprehend why different diastereomers of metal compounds are showing differences in reactivity that sometimes cannot be justified by simple steric effects. In order to study the effect of stereochemistry on the electronic structure around the metal center, RXES technique was used [38]. Two chiral platinum (II) compounds [39], namely (1S,2S)- and (1R,2R)-1-(4-fluorophenyl)-3-

isopropyl-1,2-diaminedichloro platinum(II) (*trans* and *cis*, respectively), were studied. *Cis* isomer exhibits 50-times higher anticancer activity than the *trans* one [39]. Pt L_3-edge RXES spectra of the studied samples were collected with the use of wavelength-dispersive X-ray spectrometer in von Hamos geometry. The experimental setup allows the simultaneous detection of $L\alpha_1$ and valence-to-core (V2C) signals and therefore from obtained maps, HR-XAS and V2C spectra were extracted by performing cuts at RXES plane. Experimental data were complemented with theoretical FEFF9.0 calculations of orbital contribution to the measured signals. This approach gave us the information about the density of occupied and unoccupied electronic states. **Figure 3** presents the comparison of experimental results obtained for *trans* and *cis* compounds.

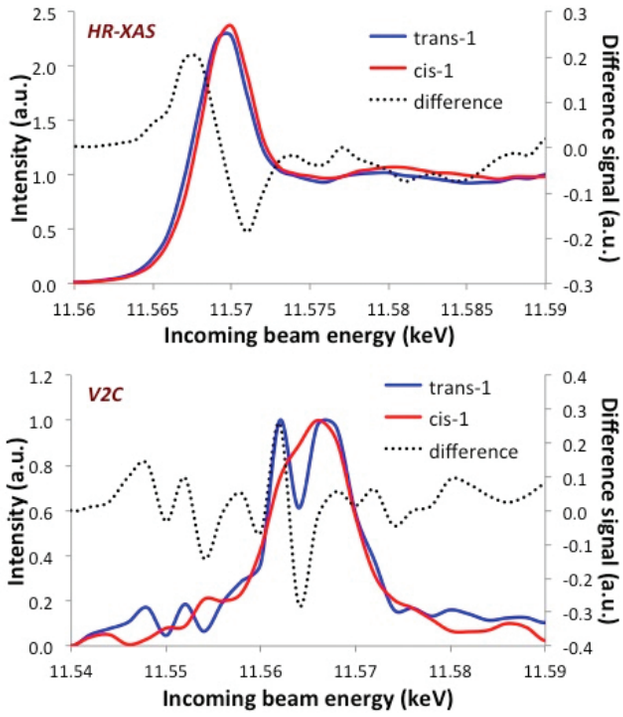

Figure 3. Comparison of the measured HR-XAS (top) and V2C emission (bottom) spectra between *trans* and *cis* Pt-derivatives. Difference profile is the result of subtracting *trans* profile from the *cis* profile [38]. Reproduced by permission of The Royal Society of Chemistry.

Calculated differential signal for both HR-XAS and V2C spectra reveals significant differences that can be associated with the increase of anticancer activity upon configuration inversion from *trans* to *cis*. In case of HR-XAS, the configuration change from *trans* to *cis* shifts the position of the white line to higher energies and increases its intensity, which is caused by increase in empty electronic states. This is related with the increase in the ability to form new bonds and strengthening the formed ones. More pronounced differences can be observed in case of V2C spectra. By analyzing the calculated orbital contributions (**Figure 4**), one can notice that two distinct peaks in V2C *trans* spectrum are resulting from the overlap of filled states of Pt-5d and Cl-2p with F-2p states forming a shoulder. In contrast, in *cis* spectrum, Pt-5d and Cl-2p do not overlap significantly and F-2p orbital is shifted toward higher energy, which results in a loss

of the shoulder and overlap of the two peaks, resolvable in case of *trans* spectrum. The same analysis was performed in order to compare the effect of substitution of various ligands in the studied compounds, and the differences in HR-XAS and V2C spectra were also observed [38] showing that changes in R^1 and R^2 positions influence Pt electronic configuration.

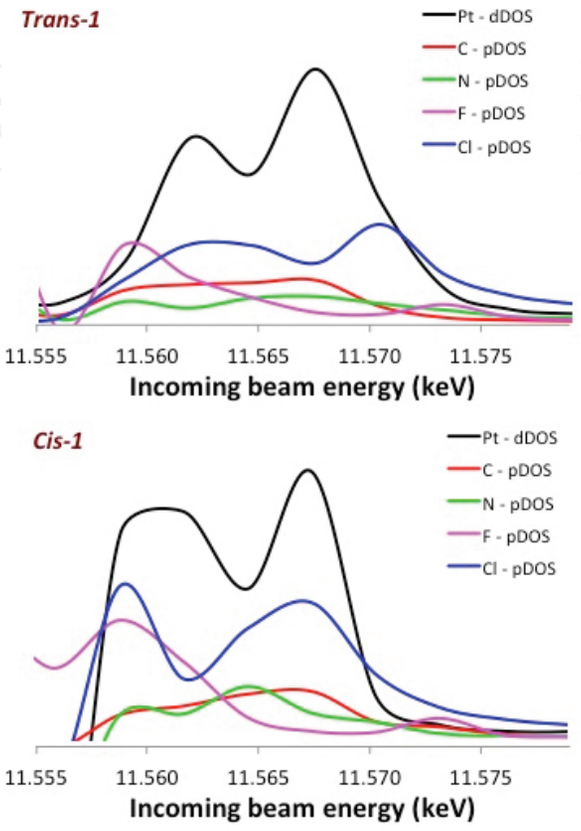

Figure 4. Orbital contribution for V2C emission spectra for *trans* and *cis* Pt-derivatives [38]. Reproduced by permission of The Royal Society of Chemistry.

As it was shown, the RXES technique is sensitive to changes of electronic structure of metallodrugs that arise not only from the changes in the structure of ligands bonded directly to the studied atom but also from the stereochemistry of further neighbors. Therefore, high chemical sensitivity of this method makes it ideal for the studies of anticancer drug mechanism in *in situ/in vivo* conditions.

3.2. The mechanism of action of chemotherapeutic drugs

In further studies, RXES method was also used to disentangle the DNA-drug interaction mechanism [7]. The studies focused on well-known cisplatin (*cis*-diamminedichloroplatinum(II)) compound that is widely used in treating a variety of cancers such as testicular, ovarian, head, and neck tumors [40]. Although very efficient, the use of cisplatin is still dose-limited by side effects and inherited or acquired resistance phenomena, only partially amended by employment of new platinum drugs [41]. Cisplatin action mechanism was only confirmed

via X-ray structural analysis to lead to the formation of intrastrand cross-links (*cis*-[$Pt(NH_3)_2${d(GpG)-N7(1),-N7(2)}]) with DNA 20 years after its implementation [42, 43].

RXES experiment was performed on cisplatin samples incubated for 24 h with calf thymus DNA. In order to follow the full mechanism of cisplatin binding, aqueous and buffer solution (physiological serum) of the drug was also studied. The intensity of the main resonance in the measured RXES Pt L_3-edge map depends directly on the unoccupancy values in the 5d orbitals, which are sensitive to the type of coordinating ligand, bonding strength and angle. Thus, changes in the structure around platinum atom can be easily detected by measuring its density of states in the 5d orbital. *In situ* RXES experiment was combined with theoretical calculations performed with FEFF9.0 code. The differential RXES maps (ΔRXES) resulting from experimental data obtained for cisplatin in aqueous and buffer solution and cisplatin incubated with DNA are presented in **Figure 5(a** and **b**). The results are compared with theoretically calculated spectra for different reaction pathways.

The analysis showed that the hydration of cisplatin in a buffer solution leads to the formation of a mono- and a diaqua complexes (*cis*-$[PtCl(NH_3)_2(H_2O)]^+$ and *cis*-$[Pt(NH_3)_2(H_2O)_2]^{2+}$, respectively). Since both complexes induce similar changes in RXES spectra, it is difficult to judge which of the structures is predominant. Nevertheless, other studies [44, 45] revealed that both structures are likely to play a role in the reaction with DNA. Further, we compare the differential RXES map resulting from the addition of calf thymus DNA to the aquated cisplatin with calculated differences. Calculations were performed for both hydration products and revealed that the final structure of cisplatin–DNA adduct is *cis*-[$Pt(NH_3)_2$-{d(GpG)-N7(1),-N7(2)}], which means that cisplatin bonds to N(7) atoms of adjacent guanines in DNA strand, which is consistent with X-ray crystallography results [42, 43]. Following step in data analysis was the extraction of HR-XAS spectra from RXES maps at constant emission energy of ~9443 eV along with FEFF9.0 calculations of orbital contributions for obtained signals (see **Figure 6**).

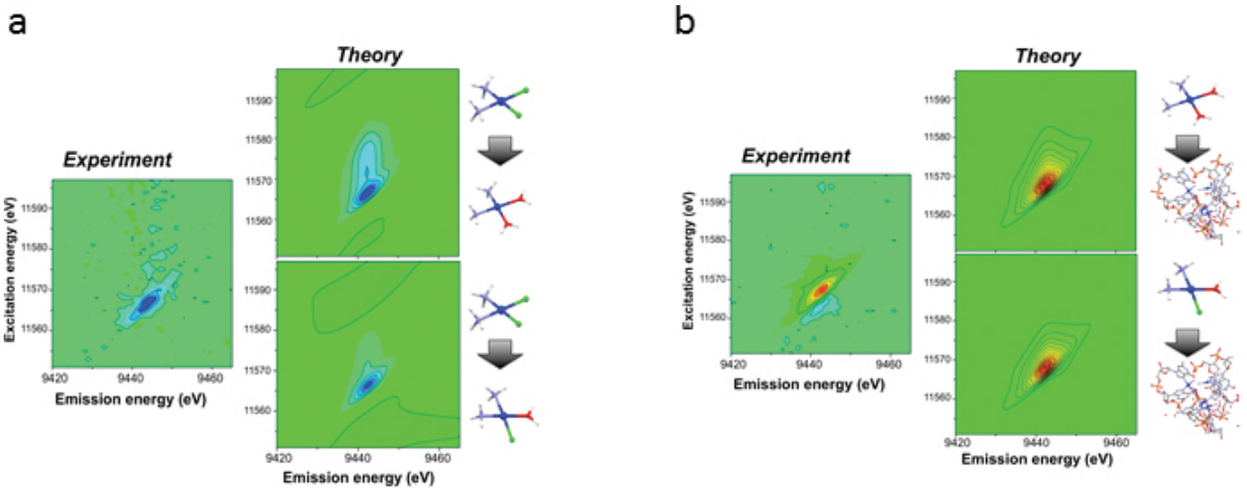

Figure 5. ΔRXES maps resulting from (a) cisplatin hydration in buffer solution. The result is compared with theoretical predictions (top) loss of two chloride ions; and (bottom) loss of a chloride ion, (b) resulting from the bonding of the aquated cisplatin with DNA. The result is compared with theoretical predictions (top) diaqua complex + DNA; and (bottom) monoaqua complex + DNA [7]. Reproduced by permission of The Royal Society of Chemistry.

http://dx.doi.org/10.5772/64953

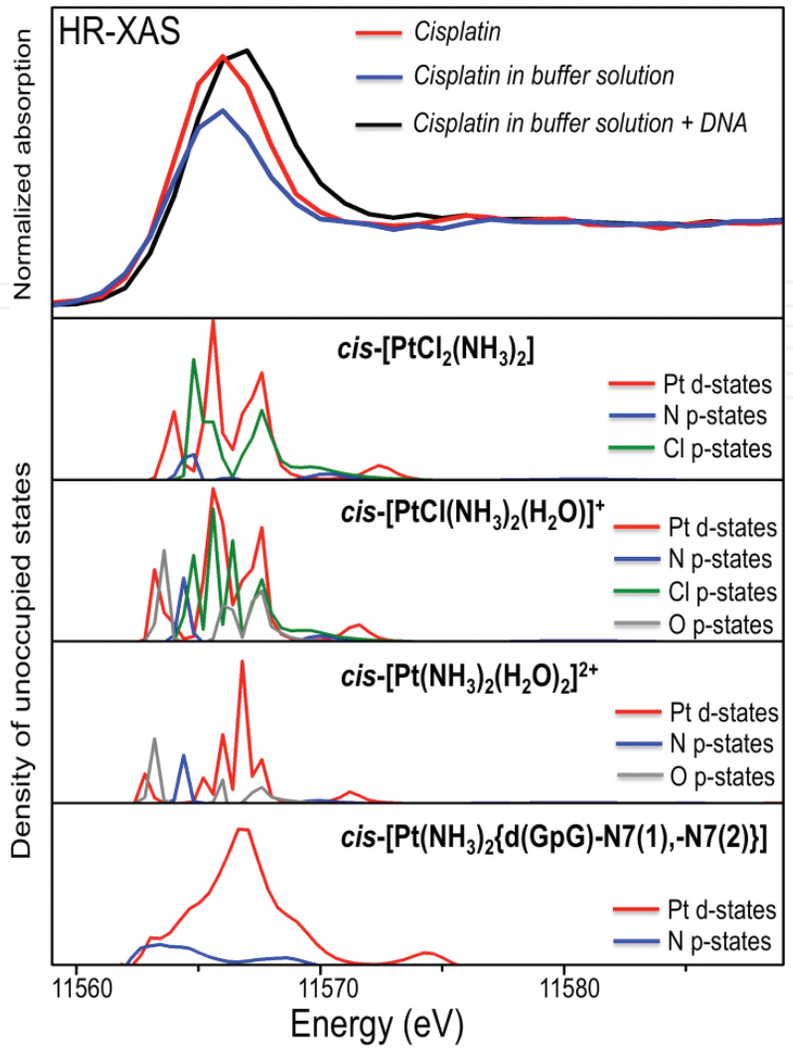

Figure 6. HR-XAS extracted from the RXES maps of (top panel) cisplatin in deionized water (red); cisplatin in buffer solution (blue); and cisplatin in buffer solution + DNA. (black). Pt 5d-density of states orbital contribution computed with FEFF9.0 (subsequent panels) [7]. Reproduced by permission of The Royal Society of Chemistry.

Changes in HR-XAS signal are clearly visible and can be interpreted by the changes in the electronic density of states of platinum and neighboring atoms. In case of hydration products, changes are associated with the substitution of Cl ligands with water molecules that lead to the removal of Cl p-orbital contribution and the appearance of a contribution due to the O p-orbitals from the water molecules that overlap less with Pt d-orbitals indicating weaker bonding. In case of cisplatin-DNA complex, HR-XAS is reflecting strong hybridization of Pt d-orbitals and p-orbitals of N(7) atoms of guanines indicating that the formed bonds are significantly stronger than Pt-Cl (cisplatin) and Pt-O (mono- and diaqua complexes).

The presented methodology has the potential to shorten the time from drug development to drug application by decades because the process is very sensitive and fairly quick, since it does not require extraction and/or preconcentration. The measurements yield direct information of bonding motifs under relevant conditions and in a time-resolved fashion. Furthermore, the

studies can be coupled with the most recent advance in theoretical calculations, which brings an even further dimension when talking about drug action mechanism understanding. RXES provides both basis and confirmation of theoretical study findings, which decreases the computational time tremendously.

We foresee this technique applied to all sorts of systems, and cells as the targets, which is enabled by X-ray probe of high penetration depth and high chemical speciation. The advent of von Hamos dispersive-type spectrometer to follow the system and improved sample delivery systems, such as liquid jet [46], ensures measurements under beam damage-free conditions.

4. Investigating DNA radiation damage

Since many years, more effort is put into the studies of the impact of radiation on human organism. Such research is carried out both in the context of radiation protection and therapy purposes. One of the most important biomolecules being strongly linked to biological radiosensitivity is DNA, which damage may trigger cell death or genomic instability. Common damage types caused by radiation are as follows: single-strand breaks (SSB) and double-strand breaks (DSB), base damage, and DNA-DNA and DNA-protein cross-links. The type and energy of radiation determine the probability of particular kinds of DNA damage production. The interactions of various kinds of radiation with DNA are complex, providing a spectrum of changes that vary in number and distribution. The molecular lesions are caused by either direct ionization/excitation of DNA or indirectly, for example, through the ionization of water and the formation of damaging-reactive hydroxyl radicals. Nevertheless, there are still unanswered questions concerning the detailed mechanism of DNA damage. For instance, the influence of low radiation doses, UV radiation, and the aspect of indirect effects is of particular interest. The biochemical and spectroscopic methods that are commonly used in these kinds of studies can identify the possible damage types and provide information about the timescale for lesion formation, but they are not directly sensitive to the lesion structure. Moreover, these methods typically involve DNA degradation, processing, staining, or labeling procedures, which by themselves may alter the DNA damage [47]. Therefore, a new experimental approach was proposed by us [48] in order to study changes in the molecular structure of the DNA backbone due to the interaction with various radiation types. Using X-ray absorption spectroscopy (XAS) at the phosphorus K-edge, the influence of radiation on both the local geometric and electronic structure around the sugar phosphate backbone was probed. The local structure around the P atoms in DNA is sensitive to the different forms of damage. The DNA strand breaks are linked to bond cleavage in the DNA backbone that can produce 5′-phosphate (5′-PO_4), 3′-phosphate (3′-PO_4), and 3′-phosphoglycolate (3′-PG) termini. Further, the formation of photolesions such as the cyclobutane pyrimidine dimer (CPD) changes the molecular conformation resulting in a distortion around the P atom. In **Figure 7**, the structure of different damage sites is presented.

http://dx.doi.org/10.5772/64953

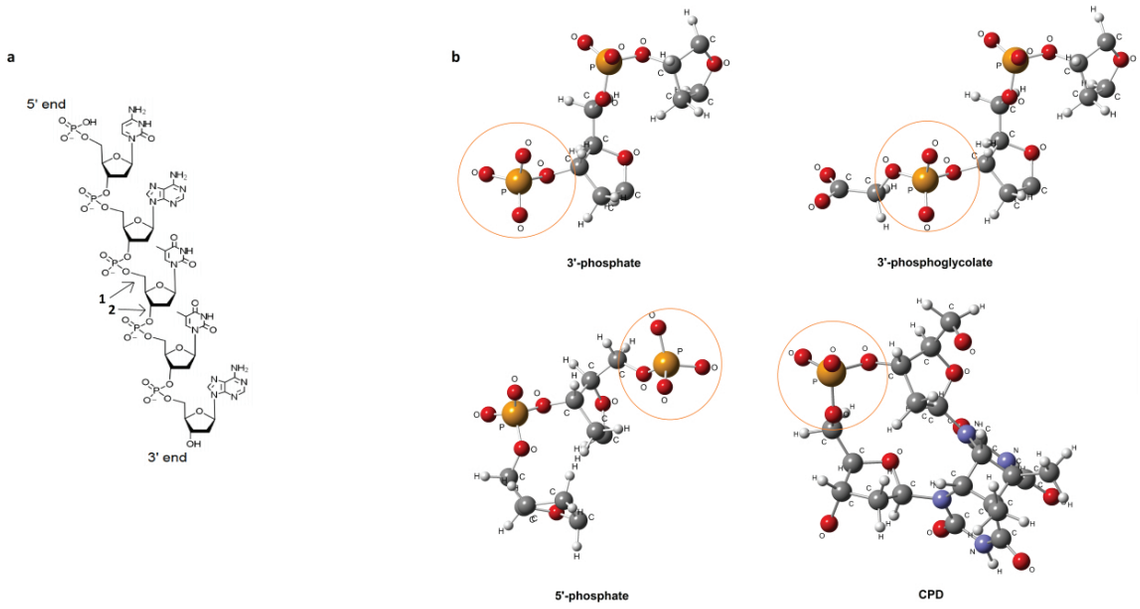

Figure 7. (a) Chemical structure of the fragment of DNA strand. Arrows indicate the bonds that can be broken and lead to 1: 3′-termini; 2: 5′-termini. (b) Structures of the four lesion types: 3′-phosphate, 3′-phosphoglycolate, 5′-phosphate, and CPD. Distorted PO_4 groups are highlighted with orange circles, reproduced from elsewhere with permission [48].

It is expected that various geometries are obtained depending on the form and energy of the radiation used. In our studies, we focused on two different radiation types, namely UV-A and proton radiation. UV-A (315–400 nm) is a main part of UV solar light that is considered as most serious environmental carcinogen. Although its absorption in DNA is rather small, it penetrates our skin very efficiently and can reach its deeper layers [49]. UV-A can cause several damage types and among them the most pronounced are single- and double-strand breaks and CPDs [50], which are produced only by UV radiation. In contrast, proton radiation produces DNA strand breaks but no CPDs. Proton radiation is the most common particle radiation used in cancer therapy of a variety of tumors, including those of the central nervous system, eye, lung, breast, prostate, head, and neck, as well as sarcomas and many pediatric cancers [51]; therefore, its detailed interaction with biomolecules has to be known.

The concept of presented studies [48] was to combine XAS experiment with theoretical calculations in order to identify the damage types and their structure. As a model sample, calf thymus DNA was used because its structure is almost identical with human DNA [52]. X-ray absorption spectra were collected for aqueous solutions of DNA irradiated with UV-A and protons, as well as for non-irradiated DNA that was used as a reference sample. Next, the spectral differences were calculated for P K-edge spectra obtained for irradiated and non-irradiated DNA (**Figure 8(a)**).

Simultaneously, P K-edge XAS spectra were calculated theoretically for each possible damage type (see structures in **Figure 7**), using FDMNES code, and the same procedure, as in case of experimental data, to obtain spectral differences was applied. Among others, the differences showed changes in the intensity of main peak in case of 3′- and 5′-phosphate that can be

associated with the break in one of the C-O bonds around PO_4 group, and a shift toward higher energies in case of CPD structure, associated with decreasing bond angle in O-P-O bond. Next, experimental differences were fitted with theoretical ones. The results of the fit for UV-A irradiated DNA are shown in **Figure 8(b)**. It was shown that the experimental difference can be reconstructed by the combination of theoretical spectra of 3′-phosphate, CPD, and 5′-phosphate with relative ratios 56% (±6.2%), 32% (±12%), and 12% (±6.8%), respectively. It indicates that the major damage types are strand breaks with predominant 3′-phosphate termini structure. Second group of damage is the formation of CPDs, which presence confirms direct absorption of UV-A radiation by DNA molecule. In case of the spectra obtained for proton-irradiated DNA, the same analysis was performed and it revealed that protons produce mainly 3′-phosphate (74% ± 17.6%) and 5′-phosphate (26% ± 19.6%) lesions. No CPDs were detected, supportive with the fact that they are only produced by UV radiation. The results for both irradiation types show that the bond between 5′-carbon atom of deoxyribose and oxygen in the phosphate group is most likely to be broken in the DNA backbone.

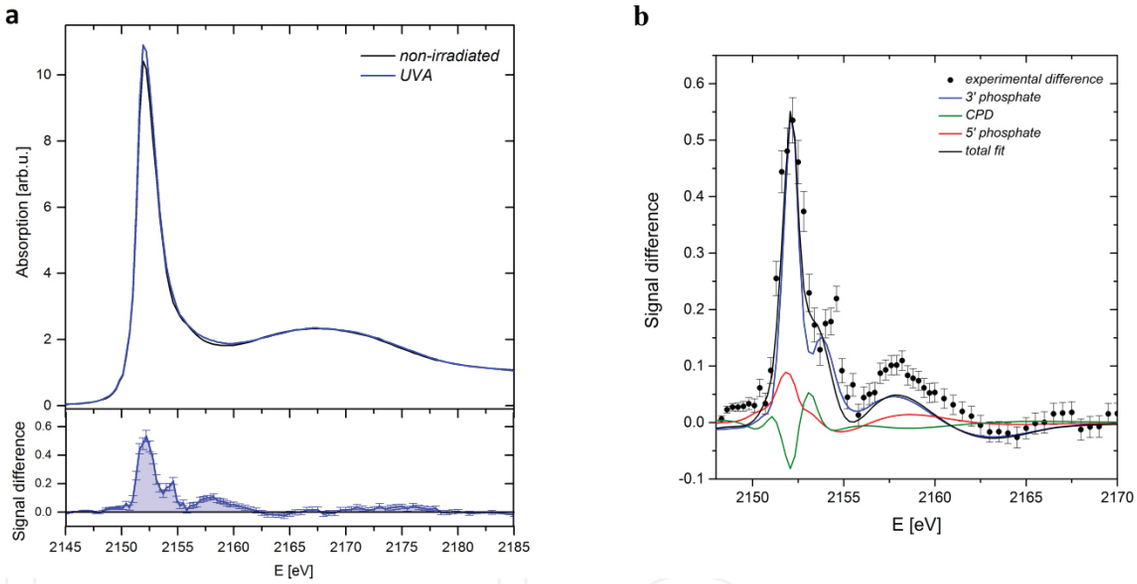

Figure 8. (a) (top) Phosphorus K-edge x-ray absorption spectra of intact and UVA-irradiated aqueous DNA samples; (bottom) P K-edge XAS difference signal between the spectrum of damaged and reference DNA sample. (b) The experimental difference of P K-edge XAS obtained for UVA-irradiated DNA sample fitted with the theoretical spectra. Reproduced from elsewhere with permission [48].

The foregoing approach of determining DNA damage can be easily implemented to study the effect of any damaging agents like various radiation types and chemical compounds. As it was shown, XAS is sensitive to the structure of the produced damage and can provide information about their relative ratios; therefore, it can be used in studies revealing the mechanism of damage development. Especially, it is important to study first stages of damage formation, since, as Boudaïffa et al. [53] suggested, "it is only through a complete understanding of such early events in the generation of genotoxic damage that we may hope to eventually manipulate the effects of ionizing radiation at a molecular level." It is foreseen that the developed methodology can be used in the time-resolved experiments on lesion formation at the X-ray free

electron lasers (XFELs), which give the opportunity to perform X-ray spectroscopy studies with ultrafast timescales.

5. Studies of changes in chemical forms of sulfur in case of prostate cancer

According to the World Health Organization, "cancer is the uncontrolled growth of cells, which can invade and spread to distant sites of the body. Cancer can have severe health consequences and is a leading cause of death" [20]. It comprises 13% of all deaths worldwide and among more than 100 types of cancerous diseases, each requiring unique diagnostic and treatment; prostate cancer is the second most common type in men [20]. As in the case of other cancerous diseases, one of the main issues in prostate cancer research is represented by the discovery and validation of new cancer biomarkers to understand its etiopathology for both diagnosis and new therapies design. A biomarker of cancer can be any structural and/or functional detectable change connected with a cancer disease in human individuals, for example, in genes, proteins, or metabolites [54]. Ideal experimental method to identify such changes should be highly sensitive, specific, and characterized by as minimal as possible sample manipulation. The studies presented in this section take advantage of X-ray spectroscopy to study sulfur species in prostate cancer cell lines and tissue [6, 8, 55, 56]. Sulfur is a key element in human organism. In biological systems, sulfur is present in all of its oxidation state from the reduced one (-2) to the most oxidized one (+6). First of all, it is a part of two amino acids—cysteine and methionine—and their derivatives, which are building blocks of many important proteins. Further, another important compound is the major low-molecular-weight thiol glutathione (GSH), which is involved in the defense against reactive oxygen species that disrupts homeostasis as observed in several pathological conditions [57]. In its oxidized form, sulfur is present for example in sulfates, like chondroitin sulfate, the glucosaminoglycan (GAG) occurring in extracellular matrix that affects proliferation and cell division during growth and differentiation of tissues. Increased expression of chondroitin sulfate is associated with the development of malignant lesions in various tissues, and it was shown that in case of prostate cancer, it indicates high tumor malignancy [58, 59]. Additionally, sulfenic, sulfinic, and sulfonic derivatives may be formed during severe oxidation stress that is strongly associated with cancerogenesis and their presence in prostate cells or their surrounding may indicate dysregulated redox balance [60]. Because of its sensitivity, X-ray absorption spectroscopy accompanied by careful data analysis was applied to such a complex and heterogenic samples.

5.1. Sulfur speciation in prostate cancer cell lines

Commercially available cell lines are often used as a model sample in different cancer research. In the first part of our experiment, three commercial prostate cancer cell lines and one non-cancerous cell lines were used. They were as follows: PC-3 cell line, derived from advanced androgen independent bone metastasized prostate cancer; DU145 cell line, derived from brain metastasis; LNCaP (androgen-sensitive human prostate adenocarcinoma cells), derived from the left supraclavicular lymph node metastasis; and PZ-HPV-7, derived from epithelial cells cultured from normal tissue obtained from the peripheral zone of the prostate. Sulfur K-edge

X-ray absorption spectra were acquired on the paraffin-fixed, dried layer of cells, placed on Mylar foil. Typical spectra obtained for each cell type are presented in **Figure 9(a)**.

All of the spectra are characterized by two strong features at energies 2472.4 and 2480.0 eV that, after the comparison with the spectra of reference compounds [6], were identified as the signature of reduced and oxidized forms of sulfur. Although the positions of the main features are identical in all spectra, they differ by the intensity. Preliminary analysis performed with the use of peak fitting method to determine the area under the peaks showed that the content of reduced sulfur forms does not vary much between cell lines but significant differences are present in the content of oxidized sulfur forms between cancerous and non-cancerous cells [6, 8]. These preliminary results suggested that there might be changes in redox balance, and therefore, the detailed analysis by linear combination fit method was performed with the use of ATHENA software [61]. The method was used before, for example, to establish sulfur forms in erythrocytes and plasma [15]. Experimental S K-edge XAS spectra of prostate cells were fitted with spectra of model sulfur-bearing compounds that are likely to be present in human cells. The chosen groups were as follows: amino acids, thiols, disulfides, sulfonates, and sulfates. In case of sulfonates, two model compounds were used: taurine and cysteic acid. The representative result of fitting procedure is shown in **Figures 9(b)** and **10** presents the results of the fitting for all cell line types in the form of bar graphs together with standard deviation.

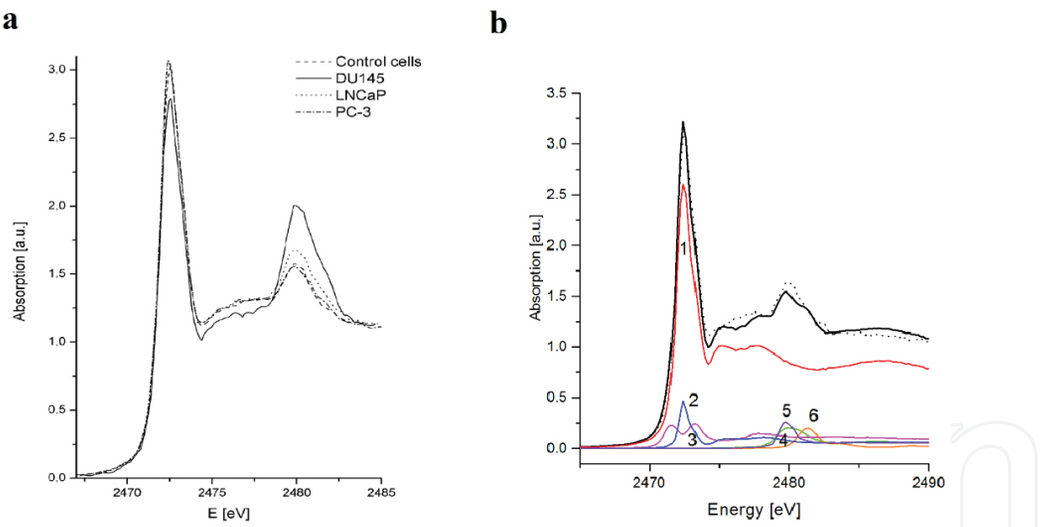

Figure 9. (a) The comparison of experimental S K-edge XANES spectra of four different cell lines. (b) Example of experimental sulfur K-edge XANES spectrum (PC3 cells, dotted line) with a linear combination (solid thick line) of: 1. amino acid, 2. thiol, 3. disulfide, 4. sulfonate (cysteic acid), 5. sulfonate (taurine), and 6. sulfate. Reproduced from elsewhere with permission [8].

In case of disulfide group, no differences were observed. There were very slight changes in amino acids and sulfates content, and the most pronounced differences were shown in case of thiols and sulfonates, especially between DU-145 cells and control cells. Thiols group may be associated mainly with reduced glutathione (GSH) and presented results for this group are consistent with the studies of Canada et al. [62] in which it was shown that DU-145 cells, in

http://dx.doi.org/10.5772/64953

comparison with other prostate cancer cells, are characterized by the highest level of GSH. GSH is known as a neutralizing agent of oxidizing species, produced during severe oxidative stress that is considered as one of the major factors in development and progression of prostate cancer [63]. The higher content might be also the indicator of active cell proliferation as it is observed in cells with aggressive phenotype [64]. The sulfonates group consists mainly of the metabolic products generated during the oxidation of cysteine. The other example is glutathione sulfonate (GSA) that is formed as a result of the interaction between reduced glutathione and free radicals [65].

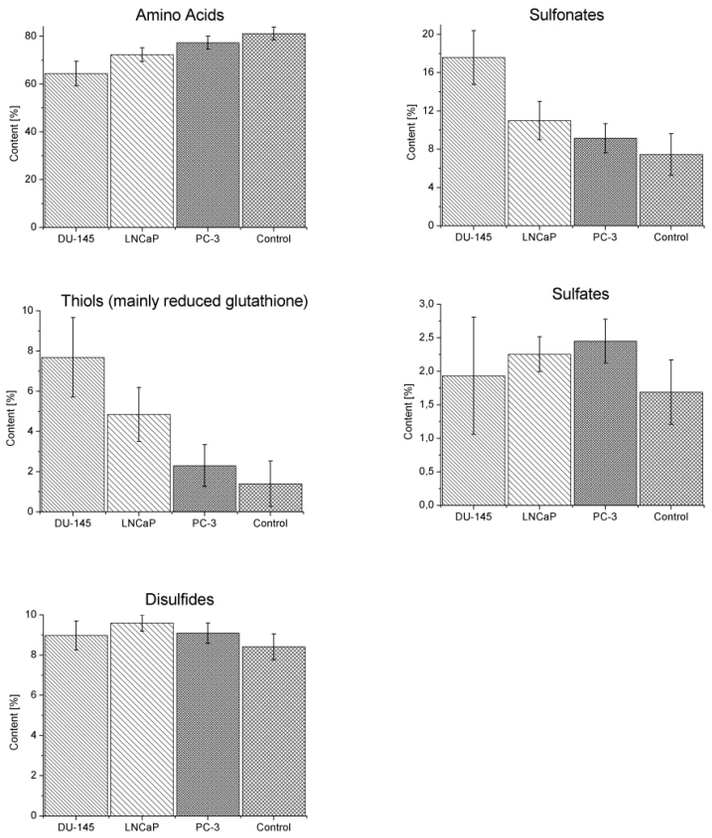

Figure 10. The content of the model groups of compounds in different cell lines obtained from linear combination fit. The sulfonate content represents both cysteic acid and taurine content. The error bars were calculated as the standard deviation of the determined mean values. Reproduced from elsewhere with permission [8].

The results obtained during the analysis of S K-edge XAS spectra of prostate cell lines gave insights into the potential biochemical changes that occur in cancer cells. The differences in the content of thiols between various cancerous cell lines and non-cancerous one may indicate a greater free radical production in cancer cells and their increased proliferative activity. Clearly visible is also the increase in the content of oxidized sulfur forms in case of cancer cells that indicates the unbalanced redox status. Although it is not clear whether these differences are a cause or consequence of malignant transformation, however, the results point out that this process influences strongly the biochemistry of sulfur-bearing compounds inside the cell.

5.2. Distribution of different forms of sulfur in prostate cancer tissue

In prostate tissue, as in other tissues in human organism, we can find different types of cells accompanied by extracellular matrix. Typical prostate is built of two main parts: prostatic glands and stroma composed from smooth muscle cells and connective tissue. Therefore, such a structure is far more complex than cell lines, in which all cells are of the same phenotype. To analyze the distribution of different forms of the element of interest in tissue, XAS imaging can be used and data need to be collected from the tissue area that covers different histological parts. The method is based on the fact that different oxidation states of the same element can be selectively excited by tuning the incidence energy. The generated fluorescence signal is collected in point-by-point mode in the chosen sample area for each of the incidence energy. The fraction of individual forms of the element can be extracted for each pixel by applying the procedure described by Pickering et al. [66, 67]. The calculated relative concentrations can then be used to generate 2D maps of the distribution of each form and compared with microscopic image.

Our experiment [56] was performed on the tissue sections obtained during routine prostatectomies that were in a form of 15-μm-thick air-dried slices placed on Mylar foil. The first step was to measure full XAS spectra in few different points on the tissue in order to establish the value of incidence energies that should be used in XAS imaging. The examples of spectra are presented in **Figure 11**.

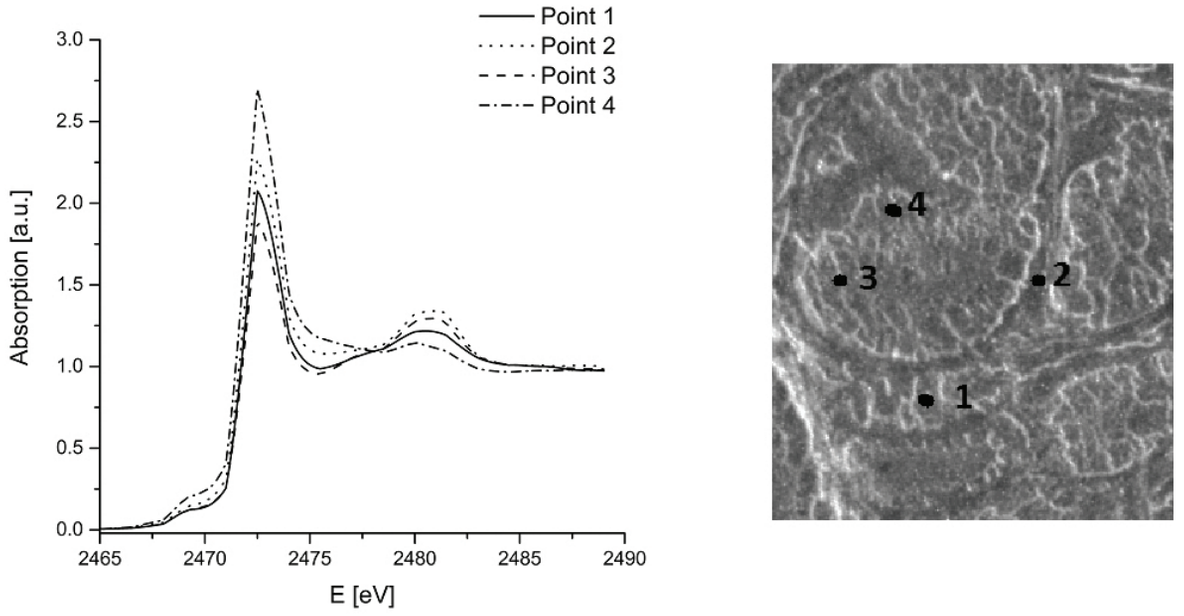

Figure 11. Sulfur K-edge μ-XANES spectra collected at different points in prostate tissue (left) together with the microscopic image of the tissue with marked measurements points (right). Spectra 1, 3, and 4 are measured in nodular part while spectrum 2 in stroma. Reproduced from elsewhere with permission [56].

The two main features have the same energy position as the ones in prostate cancer cells. Therefore, the scanning energies were set above these features (2473 and 2482 eV) to image

reduced and oxidized forms of sulfur in the tissue. Additionally, scans were also performed with energy 2477 eV, which is exciting energy of sulfur with intermediate oxidation state and 2500 eV, which excites total sulfur in the sample. The latter was used to normalize measured fluorescence intensities for different pixels. The data for prostate cancer tissue were collected with 10-μm spatial resolution that was enough to analyze different histological parts. 2D distribution maps of individual chemical forms of sulfur in three prostate cancer tissue samples obtained from three different patients are presented in **Figure 12**. Maps are accompanied by the microscopic image of the studied area.

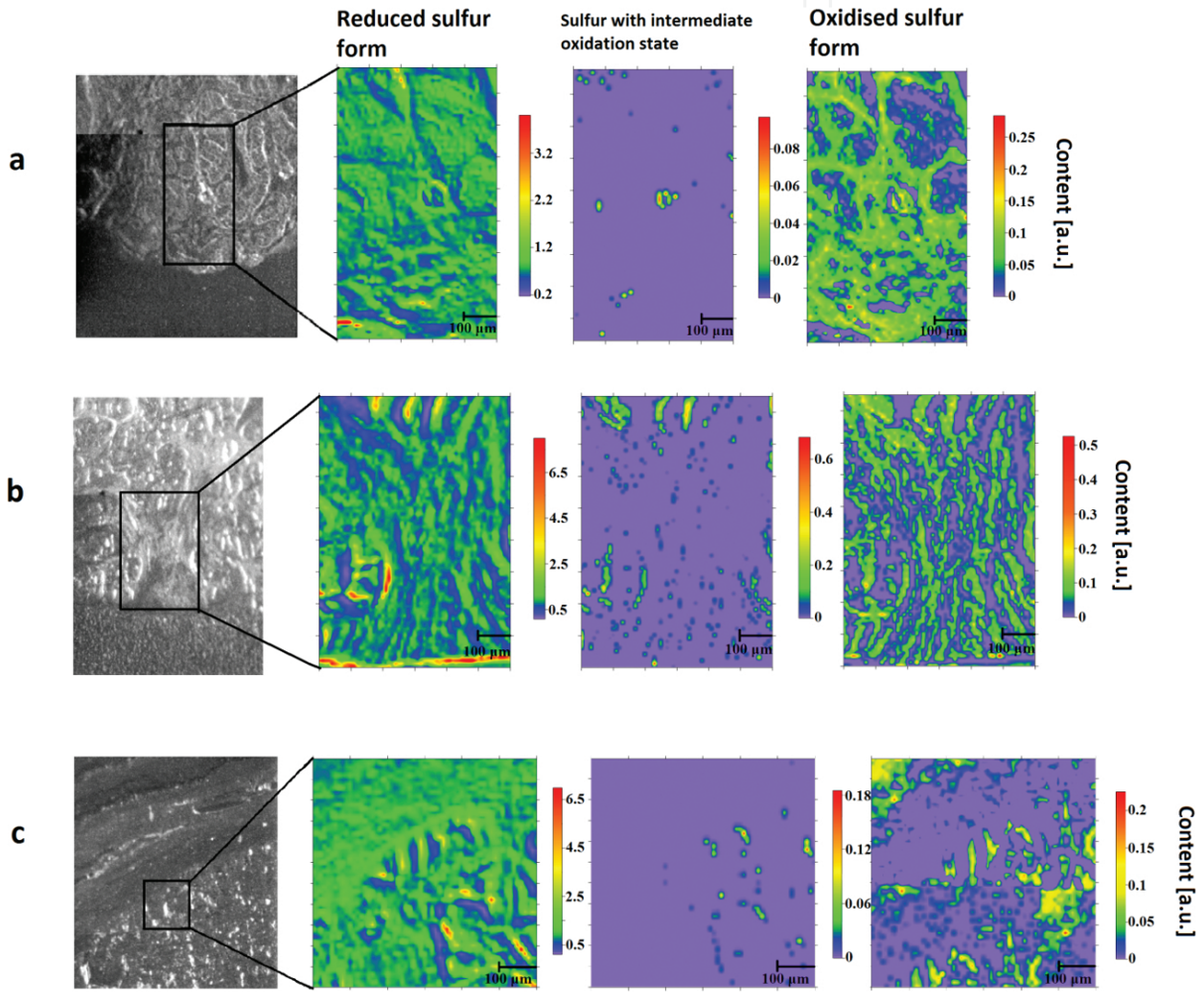

Figure 12. Two-dimensional maps of the distribution of individual chemical forms of sulfur in the selected areas of three different prostate cancer tissue slices together with microscopic image with marked area of scanning. (a–c) Samples derived from three different patients diagnosed with prostate cancer undergoing prostatectomy. Reproduced from elsewhere with permission [56].

Based on the results, we observed that the majority of sulfur located in prostate tissue occurs in reduced form, which is consistent with the results obtained for cell lines. This form is present

in all histological structures but predominantly in glandular part of the tissue. In contrast, the compounds containing sulfur with intermediate oxidation state occur in very small quantities in studied samples and they are not correlated with the specific histological structures. Sulfur with highest oxidation state is distributed unevenly, with higher content present in prostate stroma. As in case of prostate cancer cells, the occurrence of highly oxidized forms of sulfur may be the indicator of the production of oxidative derivatives of sulfur-bearing compounds resulting from the interaction with reactive oxygen species activity due to oxidative stress [60]. But in case of tissue structure, another source of sulfur with high oxidation state may be the elevated concentration of chondroitin sulfate in extracellular matrix, the compound that plays a potential role in aggressiveness of a tumor [58, 59].

Conclusions drawn from this experiment confirmed the results obtained for cell lines and extended them with information about spatial distribution of the various forms of sulfur in different histological parts of tissue. In case of heterogenous samples like human tissue, the methodology applied here allows to study the distribution of various chemical species of the same element without any chemical manipulation. In case of biologically essential elements, the detection of changes in their biochemistry can help to elucidate the possible mechanism of cancer development and progression.

Acknowledgements

Part of this work was supported by the Polish National Science Centre (NCN) under grant No. 2012/05/N/NZ5/00868 and by the European Community's Seventh Framework Program (FP7/2007-2013) under grant agreement No. 290605 (COFUND: PSI-FELLOW).

Author details

Joanna Czapla-Masztafiak[1,2*], Wojciech M. Kwiatek[1], Jacinto Sá[3,4] and Jakub Szlachetko[2,5]

*Address all correspondence to: joanna.czapla@ifj.pan.pl

1 Institute of Nuclear Physics, Polish Academy of Sciences, Krakow, Poland

2 Paul Scherrer Institut, Villigen, Switzerland

3 Department of Chemistry, Ångström Laboratory, Uppsala University, Uppsala, Sweden

4 Institute of Physical Chemistry, Polish Academy of Sciences, Warsaw, Poland

5 Institute of Physics, Jan Kochanowski University in Kielce, Kielce, Poland

References

[1] Szlachetko J, Sá J. Rational design of oxynitride materials: from theory to experiment. CrystEngComm. 2013;15:2583–2587. doi:10.1039/c3ce26909d

[2] Glatzel P, Bergmann U. High resolution 1s core hole X-ray spectroscopy in 3d transition metal complexes—electronic and structural information. Coord. Chem. Rev. 2005;249:65–95. doi:10.1016/j.ccr.2004.04.011

[3] Szlachetko J, Sá J, Nachtegaal M, Hartfelder U, Dousse J-C, Hoszowska J et al. Real time determination of the electronic structure of unstable reaction intermediates during Au_2O_3reduction. J. Phys. Chem. Lett. 2014;5:80–84. doi:10.1021/jz402309s

[4] Schäfer T, Buckau G, Artinger R, Kim JI, Geyer S, Wolf M et al. Origin and mobility of fulvic acids in the Gorleben aquifer system: implications from isotopic data and carbon/sulfur XANES. Org. Geochem. 2005;36:567–582. doi:10.1016/j.orggeochem.2004.10.011

[5] Nakai I, Matsunaga M, Adachi M, Hidaka K-I. Application of XAFS in archaeology. Journal de Physique IV Colloque. 1997;7:pp. C2-1033 – C2-1034. doi:10.1051/jp4:19972131

[6] Czapla J, Kwiatek WM, Lekki J, Steininger R, Göttlicher J. Determination of changes in sulphur oxidation states in prostate cancer cells. Acta Phys. Pol. A. 2012;121:497–501. doi:10.12693/APhysPolA.121.497

[7] Lipiec E, Czapla J, Szlachetko J, Kayser Y, Kwiatek W, Wood B, et al. Novel *in situ* methodology to observe the interactions of chemotherapeutical Pt drugs with DNA under physiological conditions. Dalton Trans. 2014;43:13839–44. doi:10.1039/c4dt00861h

[8] Czapla J, Kwiatek WM, Lekki J, Dulińska-Litewka J, Steininger R, Göttlicher J. Chemical species of sulfur in prostate cancer cells studied by XANES spectroscopy. Rad. Phys. Chem. 2013;93:154–159. doi:10.1016/j.radphyschem.2013.05.021

[9] Stone KL, Behan RK, Green MT. X-ray absorption spectroscopy of chloroperoxidase compound I: insight into the reactive intermediate of P450 chemistry. Proc. Natl. Acad. Sci. U.S.A. 2005;102:16563–16565. doi:10.1073/pnas.0507069102

[10] Salt DE, Prince RC, Baker AJM, Raskin I, Pickering IJ. Zinc ligands in the metal hyperaccumulator Thlaspi caerulescens as determined using X-ray absorption spectroscopy. Environ. Sci. Technol. 1999;33:713–717. doi:10.1021/es980825x

[11] Arcovito A, Benfatto M, Cianci M, Hasnain SS, Nienhaus K, Nienhaus GU, et al. X-ray structure analysis of a metalloprotein with enhanced active-site resolution using *in situ* X-ray absorption near edge structure spectroscopy. Proc. Natl. Acad. Sci. U. S. A. 2007;104:6211–6216. doi:10.1073/pnas.0608411104

[12] Wandzilak A, Czyzycki M, Wrobel P, Szczerbowska-Boruchowska M, Radwanska E, Adamek D, et al. The oxidation states and chemical environments of iron and zinc as

potential indicators of brain tumour malignancy grade—preliminary results. Metallomics. 2013;5:1547–1553. doi:10.1039/c3mt00158j

[13] Czapla-Masztafiak J, Lis GJ, Gajda M, Jasek E, Czubek U, Bolechała F, et al. Determination of oxidation state of iron in normal and pathologically altered human aortic valves. Nucl. Instruments Methods Phys. Res. Sect. B. 2015;364:70–75. doi:10.1016/j.nimb.2015.04.026

[14] Chwiej J, Adamek D, Szczerbowska-Boruchowska M, Krygowska-Wajs A, Bohic S, Lankosz M. Study of Cu chemical state inside single neurons from Parkinson's disease and control substantia nigra using the micro-XANES technique. J. Trace Elem. Med. Biol. 2008;22:183–188. doi:10.1016/j.jtemb.2008.03.006

[15] Pickering IJ, Prince RC, Divers T, George GN. Sulfur K-edge X-ray absorption spectroscopy for determining the chemical speciation of sulfur in biological systems. FEBS Lett. 1998;441:11–14. doi:10.1016/S0014-5793(98)01402-1

[16] Weekley CM, Aitken JB, Vogt S, Finney L a., Paterson DJ, De Jonge MD, et al. Uptake, distribution, and speciation of selenoamino acids by human cancer cells: X-ray absorption and fluorescence methods. Biochemistry. 2011;50:1641–1650. doi:10.1021/bi101678a

[17] Bacquart T, Deves G, Ortega R. Direct speciation analysis of arsenic in sub-cellular compartments using micro-X-ray absorption spectroscopy. Environ. Red. 2010;110:413–416. doi:10.1016/j.envres.2009.09.006

[18] Dau H, Haumann M. Time-resolved X-ray spectroscopy leads to an extension of the classical S-state cycle model of photosynthetic oxygen evolution. Photosynth. Res. 2007;92:327–343. doi:10.1007/s11120-007-9141-9

[19] Lima FA, Milne CJ, Amarasinghe DC V, Rittmann-Frank MH, Veen RM Van Der, Reinhard M, et al. A high-repetition rate scheme for synchrotron-based picosecond laser pump X-ray probe experiments on chemical and biological systems in solution. Rev. Sci. Instrum. 2011;82:063111. doi:10.1063/1.3600616

[20] Available from: http://www.who.int/cancer/en/ [Accessed: 11.07.2016]

[21] Sá J. High-resolution XAS/XES: analyzing electronic strudtures of catalysis. CRC Press: Taylor and Francis Group; 2014.

[22] Lundberg M, Kroll T, DeBeer S, Bergmann U, Wilson S, Glatzel P, et al. Metal-ligand covalency of iron complexes from high-resolution resonant inelastic X-ray scattering. J. Am. Chem. Soc. 2013;135:17121–17134. doi:10.1021/ja408072q

[23] Pollock CJ, DeBeer S. Valence-to-core X-ray emission spectroscopy: a sensitive probe of the nature of a bound ligand. J. Am. Chem. Soc. 2011;133:5594–5601. doi:10.1021/ja200560z

[24] Vankó G, Renz F, Molnár G, Neisius T, Kárpáti S. Hard-X-ray-induced excited-spin-state trapping. Angew. Chemie Int. Ed. 2007;46:5306–5309. doi:10.1002/anie.200604432

[25] Bergmann U, Glatzel P. X-ray emission spectroscopy. Photosynth. Res. 2009;102:255–266. doi:10.1007/s11120-009-9483-6

[26] Sikora M, Juhin A, Weng T-C, Sainctavit P, Detlefs C, de Groot F, et al. Strong K-edge magnetic circular dichroism observed in photon-in-photon-out spectroscopy. Phys. Rev. Lett. 2010;105:037202. doi:10.1103/PhysRevLett.105.037202

[27] Singh J, Lamberti C, van Bokhoven J. Advanced X-ray absorption and emission spectroscopy: *in situ* catalytic studies. Chem. Soc. Rev. 2010;39:4754–4766. doi:10.1039/c0cs00054j

[28] Lancaster KM, Roemelt M, Ettenhuber P, Hu Y, Ribbe MW, Neese F, et al. X-ray emission spectroscopy evidences a central carbon in the nitrogenase iron-molybdenum cofactor. Science. 2011;334:974–977. doi:10.5061/dryad.6m0f6870

[29] Campbell JL, Papp T. Atomic level widths for X-ray spectrometry. X-ray Spetrom. 1995;24:307–319. doi:10.1002/xrs.1300240606

[30] Campbell JL, Papp T. Widths of the atomic K-N7 levels. At. Data Nucl. Data Tables. 2001;77:1–56. doi:10.1006/adnd.2000.0848

[31] von Hámos L. X-ray spectroscopy and imaging by means of a curved crystal reflectors. Naturwissenschaften. 1932;20:705.

[32] Hoszowska J, Dousse JC, Kern J, Rheme C. High-resolution von Hamos crystal X-ray spectrometer. Nucl. Instrum. Methods Phys. Res. Sect. A. 1996;376:129–138. doi:10.1016/0168-9002(96)00262-8

[33] Johannson T. On a novel, exactly focusing X-ray spectrometer. Zeitschrift Für Phys. 1931;82:507.

[34] Johann HH. Obtaining intense X-ray spectra by means of concave crystals. Zeitschrift Für Phys. 1931;69:185.

[35] Szlachetko J, Nachtegaal M, De Boni E, Willimann M, Safonova O, Sà J, et al. A von Hamos X-ray spectrometer based on a segmented-type diffraction crystal for single-shot X-ray emission spectroscopy and time-resolved resonant inelastic X-ray scattering studies. Rev. Sci. Instrum. 2012;83:103105. doi:10.1063/1.4756691

[36] Rehr JJ, Kas JJ, Vila FD, Prange MP, Jorissen K. Parameter-free calculations of X-ray spectra with FEFF9. Phys. Chem. Chem. Phys. 2010;12:5503–5513. doi:10.1039/b926434e

[37] Bunău O, Joly Y. Self-consistent aspects of X-ray absorption calculations. J. Phys. Condens. Matter. 2009;21:345501. doi:10.1088/0953-8984/21/34/345501

[38] Sá J, Czapla-Masztafiak J, Lipiec E, Kayser Y, Fernandes DLA, Szlachetko J, et al. Resonant X-ray emission spectroscopy of platinum(ii) anticancer complexes. Analyst. 2016;141:1226–1232. doi:10.1039/C5AN02490K

[39] Berger G, Leclercqz H, Derenne A, Gelbcke M, Goormaghtigh E, Nève J, et al. Synthesis and in vitro characterization of platinum(II) anticancer coordinates using FTIR spectroscopy and NCI COMPARE: a fast method for new compound discovery. Bioorg. Med. Chem. 2014;22:3527–3536. doi:10.1016/j.bmc.2014.04.017

[40] Tisato F, Marzano C, Porchia M, Pellei M, Santini C. Copper in diseases and treatments, and copper-based anticancer strategies. Med. Res. Rev. 2010;30:708–749. doi:10.1002/med.20174

[41] Santini C, Pellei M, Gandin V, Porchia M, Tisato F, Marzano C. Advances in copper complexes as anticancer agents. Chem. Rev. 2014;114:815–862. doi:10.1021/cr400135x

[42] Sherman SE, Gibson D, Wang AH-J, Lippard SJ. X-ray structure of the major adduct of the anticancer drug cisplatin with DNA: cis-[Pt(NH3)2(d(pGpG))]. Science. 1985;230:412–417. doi:10.1126/science.4048939

[43] Takahara P, Rosenzweig A, Frederick C, Lippard S. Crystal structure of double-stranded DNA containing the major adduct of the anticancer drug cisplatin. Nature. 1995;377:649–652. doi:10.1038/377649a0

[44] Baik MH, Friesner RA, Lippard SJ. Theoretical study of cisplatin binding to purine bases: why does cisplatin prefer guanine over adenine? J. Am. Chem. Soc. 2003;125:14082–14092. doi:10.1021/ja036960d

[45] Cepeda V, Fuertes M, Castilla J, Alonso C, Quevedo C, Pérez JM. Biochemical mechanisms of cisplatin cytotoxicity. Anticancer. Agents Med. Chem. 2007;7:3–18. doi:10.2174/187152007779314044

[46] Fernandes DLA, Pavliuk MV, Sá J. A 3D printed microliquid jet with an adjustable nozzle diameter. Analyst. 2015;140:6234–6238. doi:10.1039/C5AN01329A

[47] Jiang Y, Rabbi M, Kim M, Ke C, Lee W, Clark RL, et al. UVA generates pyrimidine dimers in DNA directly. Biophys J. 2009;96:1151–1158. doi:10.1016/j.bpj.2008.10.030

[48] Czapla-Masztafiak J, Szlachetko J, Milne CJ, Lipiec E, Sá J, Penfold TJ, et al. Investigating DNA radiation damage using X-ray Absorption Spectroscopy (XAS). Biophys. J. 2016;110:1304–1311. doi:10.1016/j.bpj.2016.01.031

[49] Osipov AN, Smetanina NM, Pustovalova MV, Arkhangelskaya E, Klokov D. The formation of DNA single-strand breaks and alkali-labile sites in human blood lymphocytes exposed to 365-nm UVA radiation. Free Radic. Biol. Med. 2014;73:34–40. doi:10.1016/j.freeradbiomed.2014.04.027

[50] Kielbassa C, Roza L, Epe B. Wavelength dependence of oxidative DNA damage induced by UV and visible light. Carcinogenesis. 1997;18:811–816. doi:10.1093/carcin/18.4.811

[51] Foote RL, Stafford SL, Petersen IA, Pulido JS, Clarke MJ, Schild SE, et al. The clinical case for proton beam therapy. Radiat. Oncol. 2012;7:174–183. doi:10.1186/1748-717X-7-174

[52] Mouret S, Philippe C, Gracia-Chantegrel J, Banyasz A, Karpati S, Markovitsi D, et al. UVA-induced cyclobutane pyrimidine dimers in DNA: a direct photochemical mechanism? Org. Biomol. Chem. 2010;8:1706–1711. doi:10.1039/b924712b

[53] Boudaïffa B, Cloutier P, Hunting D, Huels M a, Sanche L. Resonant formation of DNA strand breaks by low-energy (3 to 20 eV) electrons. Science. 2000;287:1658–1660. doi:10.1126/science.287.5458.1658

[54] Bellisola G, Sorio C. Infrared spectroscopy and microscopy in cancer research and diagnosis. Am. J. Cancer Res. 2012;2:1–21.

[55] Kwiatek WM, Czapla J, Podgórczyk M, Kisiel A, Konior J, Balerna A. First approach to studies of sulphur electron DOS in prostate cancer cell lines and tissues studied by XANES. Rad. Phys. Chem. 2011;80:1104–1108. doi:10.1016/j.radphyschem.2011.05.005

[56] Czapla-Masztafiak J, Okoń K, Gałka M, Huthwelker T, Kwiatek WM. Investigating the distribution of chemical forms of sulfur in prostate cancer tissue using X-ray absorption spectroscopy. Appl. Spectrosc. 2016;70:264–271. doi:10.1177/0003702815620128

[57] Matés JM, Segura JA, Alonso FJ, Márquez J. Pathways from glutamine to apoptosis. Front. Biosci. 2006;11:3164–3180.

[58] Ricciardelli C, Mayne K, Sykes PJ, Raymond WA, McCaul K, Marshall VR, et al. Elevated stromal chondroitin sulfate glycosaminoglycan predicts progression in early-stage prostate cancer. Clin. Cancer Res. 1997;3:983–992.

[59] Ricciardelli C, Quinn DI, Raymond WA, McCaul K, Sutherland PD, Stricker PD, et al. Elevated levels of peritumoral chondroitin sulfate are predictive of poor prognosis in patients treated by radical prostatectomy for early-stage prostate cancer. Cancer Res. 1999;59:2324–2328.

[60] Paschos A, Pandya R, Duivenvoorden WCM, Pinthus JH. Oxidative stress in prostate cancer: changing research concepts towards a novel paradigm for prevention and therapeutics. Prostate Cancer Prostatic Dis. 2013;16:217–225. doi:10.1038/pcan.2013.13

[61] Ravel B, Newville M. ATHENA, ARTEMIS, HEPHAESTUS: data analysis for X-ray absorption spectroscopy using IFEFFIT. J. Synchrotron Radiat. 2005;12:537–541. doi:10.1107/S0909049505012719

[62] Canada AT, Roberson KM, Vessella RL, Trump DL, Robertson CN, Fine RL. Glutathione and glutathione S-transferase in benign and malignant prostate cell lines and prostate tissues. Biochem. Pharmacol. 1996;51:87–90. doi:10.1016/0006-2952(95)02157-4

[63] Khandrika L, Kumar B, Koul S, Maroni P, Koul HK. Oxidative stress in prostate cancer. Cancer Lett. 2009;282:125–136. doi:10.1016/j.canlet.2008.12.011

[64] Matés JM, Pérez-Gómez C, De Castro IN, Asenjo M, Márquez J. Glutamine and its relationship with intracellular redox status, oxidative stress and cell proliferation/death. Int. J. Biochem. Cell Biol. 2002;34:439–458. doi:10.1016/S1357-2725(01)00143-1

[65] Wefers H, Sies H. Oxidation of glutathione by the superoxide radical to the disulfide and the sulfonate yielding singlet oxygen. Eur. J. Biochem. 1983;137:29–36.

[66] Pickering IJ, Sneeden EY, Prince RC, Block E, Harris HH, Hirsch G, et al. Localizing the chemical forms of sulfur in vivo using X-ray fluorescence spectroscopic imaging: application to onion (*Allium cepa*) tissues. Biochemistry. 2009;48:6846–6853. doi:10.1021/bi900368x

[67] Pickering IJ, George GN. X-ray absorption spectroscopy imagin of biological tissues. AIP Conf. Proc. 2007;882:311–315. doi:10.1063/1.2644509